

Model-free Adaptive Output Feedback Vibration Suppression in a Cantilever Beam

Juan Augusto Paredes Salazar*, Ankit Goel†

This paper presents a model-free adaptive control approach to suppress vibrations in a cantilevered beam excited by an unknown disturbance. The cantilevered beam under harmonic excitation is modeled using a lumped parameter approach. Based on retrospective cost optimization, a sampled-data adaptive controller is developed to suppress vibrations caused by external disturbances. Both displacement and acceleration measurements are considered for feedback. Since acceleration measurements are more sensitive to spillover, which excites higher frequency modes, a filter is developed to extract key displacement information from the acceleration data and enhance suppression performance. The vibration suppression performance is compared using both displacement and acceleration measurements.

I. Introduction

Vibrations caused by external disturbances occur in several engineering applications, resulting in decreased performance and potentially leading to instability. Active vibration control techniques have been proposed to address this issue [1–7]. In particular, control vibration suppression has been applied to marine vehicles and structures for vibrations induced by machinery [8–10], building structures for vibrations induced by strong winds and earthquakes [11–13], and aerospace vehicles for vibrations in satellites and flexible wings [14–19]. Numerous techniques have been implemented for this purpose, including LQR [20–22], robust control [23–25], and adaptive control [26–31].

In this manuscript, we propose the implementation of Retrospective Cost Adaptive Control (RCAC) [32], a model-free output feedback technique, for vibration suppression. RCAC has been previously implemented to suppress oscillations in vibrational and self-excited systems [33–35]. A cantilever beam system under external disturbance is considered a testbed for its ubiquitous presence in the active vibration control literature.

The structural model considered in this paper is motivated by the cantilever beam shown in Figure 1. A bass shaker is used to harmonically excite the cantilever and the objective is to minimize the displacement at the sensor location. The input is applied by another bass shaker mounted at a different point on the cantilever. Note that the measurement, actuation, and disturbance are not colocated in this example. Both position and acceleration measurements are considered for feedback.

Since acceleration measurements are more sensitive to spillover, which results in higher frequency modes being excited by the controller [1, 36–39], a filter is developed to extract key displacement information from the acceleration data and improve suppression performance [40–44]. The vibration suppression performance of RCAC is compared using both displacement and acceleration measurements.

The contents of the paper are as follows. Section II introduces a lumped parameter model for the cantilever beam system, motivated by the cantilever beam shown in Figure 1. Section III provides an overview of the control system, including a review of RCAC, the sampled-data implementation of RCAC that interfaces the discrete-time controller with the continuous-time system, and the signal conditioning filters used for displacement and acceleration measurements. Section IV provides the results of numerical simulations in which RCAC is implemented to suppress vibrations in the lumped parameter model developed in Section II. Section V provides conclusions.

Notation: $\mathbb{R} \triangleq (-\infty, \infty)$, $\mathbb{R}^{\geq 0} \subset \mathbb{R} \triangleq [0, \infty)$, $\mathbb{Z} \triangleq \{\dots, -2, -1, 0, 1, 2, \dots\}$, and $\|\cdot\|$ denotes the Euclidean norm on \mathbb{R}^n . $x_{(i)}$ denotes the i th component of $x \in \mathbb{R}^n$. $\mathbf{q} \in \mathbb{C}$ is the forward-shift operator. For all $i \in \{1, \dots, n\}$, let $e_{n,i} \triangleq \begin{bmatrix} e_{n,i(1)} & e_{n,i(2)} & \dots & e_{n,i(n)} \end{bmatrix}^T \in \mathbb{R}^n$, such that

$$e_{n,i(j)} \triangleq \begin{cases} 1, & \text{if } i = j, \\ 0, & \text{otherwise.} \end{cases}$$

*Postdoctoral Research Fellow, Department of Mechanical Engineering, University of Maryland, Baltimore County, 1000 Hilltop Circle, Baltimore, MD 21250. japarede@umbc.edu

†Assistant Professor, Department of Mechanical Engineering, University of Maryland, Baltimore County, 1000 Hilltop Circle, Baltimore, MD 21250. ankgoel@umbc.edu

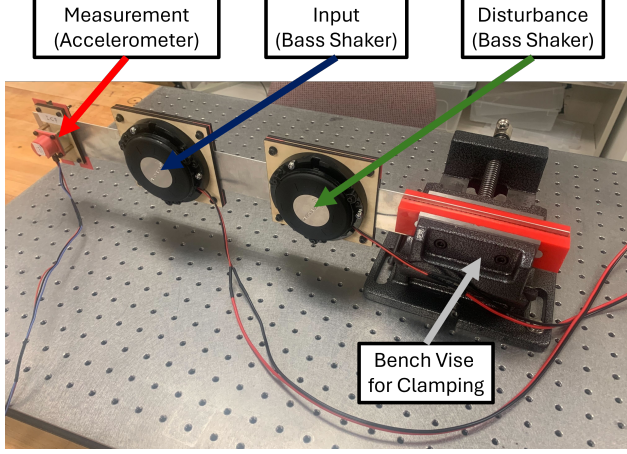


Fig. 1 Cantilever beam laboratory setup.

The symmetric matrix $P \in \mathbb{R}^{n \times n}$ is positive semidefinite (resp., positive definite) if all of its eigenvalues are nonnegative (resp., positive). $\text{vec } X \in \mathbb{R}^{nm}$ denotes the vector formed by stacking the columns of $X \in \mathbb{R}^{n \times m}$, and \otimes denotes the Kronecker product. I_n is the $n \times n$ identity matrix, $0_{n \times m}$ is the $n \times m$ zeros matrix, and $\mathbb{1}_{n \times m}$ is the $n \times m$ ones matrix.

II. Lumped Parameter Model

In this section, a lumped parameter (LP) model of a cantilever beam is derived based on the methodology shown in [45]. A LP model of a cantilever beam clamped to a wall of length L , cross-section width b , cross-section height h , and mass m is obtained by dividing the beam into n_b elements of length $\Delta L \triangleq L/n_b$, as shown in Figure 2. Let axes \hat{i} and \hat{j} be perpendicular and parallel to the wall, respectively, as shown in Figure 2, and note that the beam is aligned with \hat{i} when it is unforced. Let p_0 be the clamping point on the wall. For all $i \in \{1, \dots, n_b\}$, let p_i be the farthest point of the i -th element from p_0 , let w_i be the displacement of p_i in the direction of \hat{j} , let $w_{c,i}$ be the displacement of the center of mass of the i -th element in the direction of \hat{j} , such that

$$w_{c,i} \triangleq \begin{cases} \frac{w_1}{2}, & \text{if } i = 1, \\ \frac{w_{i-1} + w_i}{2}, & \text{if } i \in \{2, \dots, n_b\}, \end{cases} \quad (1)$$

let ϕ_i be the angle of rotation of the i -th element relative to \hat{i} , and let f_i be the external force applied to p_i in the direction of \hat{j} . Assume that $\phi_1, \dots, \phi_{n_b}$ are small. Then,

$$\phi_i = \begin{cases} \phi_1 = \frac{w_1}{\Delta L} & \text{if } i = 1, \\ \phi_i = \frac{w_i - w_{i-1}}{\Delta L} & \text{if } i \in \{2, \dots, n_b\}. \end{cases} \quad (2)$$

For all $j \in \{0, \dots, n_b - 1\}$, let the angle between adjacent elements at point p_j be given by

$$\Delta\phi_j \triangleq \begin{cases} \phi_1 = \frac{w_1}{\Delta L} & \text{if } j = 0, \\ \phi_2 - \phi_1 = \frac{w_2 - 2w_1}{\Delta L} & \text{if } j = 1, \\ \phi_{j+1} - \phi_j = \frac{w_{j+1} - 2w_j + w_{j-1}}{\Delta L} & \text{if } j \in \{2, \dots, n_b - 1\}. \end{cases} \quad (3)$$

Next, assuming that the force of gravity has no effect on the displacement of any element of the beam, the total potential energy U and the total kinetic energy T relative to p_0 are given by

$$U = \sum_{j=0}^{n_b-1} \frac{1}{2} K_\phi (\Delta\phi_j)^2, \quad (4)$$

$$T = \sum_{i=1}^{n_b} \frac{1}{2} \Delta m \dot{w}_{c,i}^2 + \frac{1}{2} J \dot{\phi}_i^2, \quad (5)$$

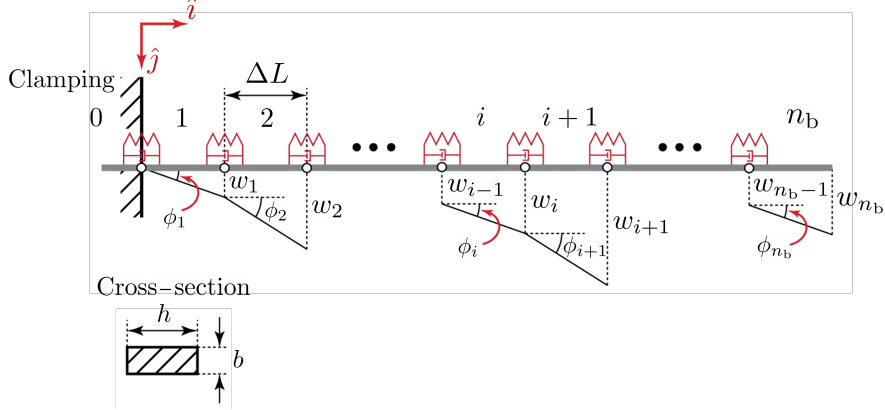


Fig. 2 Lumped parameter model of a cantilever beam.

where $\Delta m \triangleq m/n_b$, $K_\phi \triangleq \frac{Ehb^3}{4\Delta L}$, is the stiffness between each element, E is Young's modulus corresponding to the beam material, and $J \triangleq \Delta m \frac{\Delta L^2+b^2}{12}$ is the inertia of each element along an axis perpendicular to the plane. Then, it follows from (1) – (5) that, for all $i \in \{1, \dots, n_b\}$,

$$\frac{\partial U}{\partial w_i} = \begin{cases} \frac{K_\phi}{\Delta L^2} (6w_1 - 4w_2 + w_3) & \text{if } i = 1, \\ \frac{K_\phi}{\Delta L^2} (-4w_1 + 6w_2 - 4w_3 + w_4) & \text{if } i = 2, \\ \frac{K_\phi}{\Delta L^2} (w_{i-2} - 4w_{i-1} + 6w_i - 4w_{i+1} + w_{i+2}) & \text{if } i \in \{3, \dots, n_b - 2\}, \\ \frac{K_\phi}{\Delta L^2} (w_{n_b-3} - 4w_{n_b-2} + 5w_{n_b-1} - 2w_{n_b}) & \text{if } i = n_b - 1, \\ \frac{K_\phi}{\Delta L^2} (w_{n_b-2} - 2w_{n_b-1} + w_{n_b}) & \text{if } i = n_b, \end{cases} \quad (6)$$

$$\frac{\partial}{\partial t} \left(\frac{\partial T}{\partial \dot{w}_i} \right) = \begin{cases} \gamma_1 \ddot{w}_1 + \gamma_2 \ddot{w}_2 & \text{if } i = 1, \\ \gamma_2 \ddot{w}_{i-1} + \gamma_1 \ddot{w}_i + \gamma_2 \ddot{w}_{i+1} & \text{if } i \in \{2, \dots, n_b - 1\}, \\ \gamma_2 \ddot{w}_{n_b-1} + \frac{\gamma_1}{2} \ddot{w}_{n_b} & \text{if } i = n_b, \end{cases} \quad (7)$$

where

$$\gamma_1 = \frac{\Delta m}{2} \left(1 + \frac{1}{3} \left(1 + \left(\frac{b}{\Delta L} \right)^2 \right) \right), \quad \gamma_2 = \frac{\Delta m}{4} \left(1 - \frac{1}{3} \left(1 + \left(\frac{b}{\Delta L} \right)^2 \right) \right).$$

Hence, it follows from (6), (7), and the Euler-Lagrange equations that, for all $i \in \{1, \dots, n_b\}$, the equations of motion of the cantilever system are given by

$$\frac{\partial}{\partial t} \left(\frac{\partial T}{\partial \dot{w}_i} \right) + \frac{\partial U}{\partial w_i} = f_i. \quad (8)$$

Rewriting (8) into a matrix differential equation yields

$$M \ddot{w} + K w = f, \quad (9)$$

where

$$w \triangleq \begin{bmatrix} w_1 & \dots & w_{n_b} \end{bmatrix}^T, \quad f \triangleq \begin{bmatrix} f_1 & \dots & f_{n_b} \end{bmatrix}^T,$$

$$M = \begin{bmatrix} \gamma_1 & \gamma_2 & 0 & \cdots & \cdots & \cdots & \cdots & \cdots & \cdots \\ \vdots & \vdots \\ \cdots & 0 & \gamma_2 & \gamma_1 & \gamma_2 & 0 & \cdots & & \\ \vdots & \vdots \\ \cdots & \cdots & \cdots & \cdots & 0 & \gamma_2 & \frac{\gamma_1}{2} & & \end{bmatrix}, \quad K \triangleq \frac{K_\phi}{\Delta L^2} \begin{bmatrix} 6 & -4 & 1 & 0 & \cdots & \cdots & \cdots & \cdots & \cdots \\ -4 & 6 & -4 & 1 & 0 & \cdots & \cdots & \cdots & \cdots \\ \vdots & \vdots \\ \cdots & 0 & 1 & -4 & 6 & -4 & 1 & 0 & \cdots \\ \vdots & \vdots \\ \cdots & \cdots & \cdots & \cdots & 0 & 1 & -4 & 5 & -2 \\ \cdots & \cdots & \cdots & \cdots & 0 & 1 & -2 & 1 & \end{bmatrix}.$$

To account for the presence of structural damping, (9) is modified as

$$M\ddot{w} + C_R\dot{w} + Kw = f, \quad (10)$$

where $C_R \triangleq \alpha M + \beta K$ is the Rayleigh damping matrix, and $\alpha, \beta \in \mathbb{R}$ determine the damping ratios corresponding to the eigenvalues of the cantilever system matrix.

Next, let $i_u, i_d \in \{1, \dots, n_b\}$ be the beam elements at which the input and the disturbance are applied, respectively, let $u \in \mathbb{R}$ be an input force applied at p_{i_u} , and let $d \in \mathbb{R}$ be an external disturbance applied at p_{i_d} , such that

$$f = e_{n_b, i_u}u + e_{n_b, i_d}d. \quad (11)$$

Let $x \triangleq \begin{bmatrix} w^T & \dot{w}^T \end{bmatrix}^T$. Then, it follows from (10), (11) that the equations of motion of the cantilever system can be written in state space form as

$$\dot{x} = Ax + B_u u + B_d d, \quad (12)$$

where

$$A \triangleq \begin{bmatrix} 0_{n_b \times n_b} & I_{n_b} \\ -M^{-1}K & -M^{-1}C_R \end{bmatrix}, \quad B_u \triangleq \begin{bmatrix} 0_{n_b \times 1} \\ M^{-1}e_{n_b, i_u} \end{bmatrix}, \quad B_d \triangleq \begin{bmatrix} 0_{n_b \times 1} \\ M^{-1}e_{n_b, i_d} \end{bmatrix}.$$

Next, let $i_y \in \{1, \dots, n_b\}$ be the beam element from which a measurement is obtained, let $y \in \mathbb{R}$ be a measurement obtained from p_{i_y} . In the case where a displacement measurement is available, $y = w_{i_y}$, and

$$y = C_{\text{disp}}x, \quad (13)$$

where

$$C_{\text{disp}} \triangleq \begin{bmatrix} e_{n_b, i_y} & 0_{n_b \times 1}^T \end{bmatrix}^T.$$

In the case where an acceleration measurement is available, $y = \ddot{w}_{i_y}$, and

$$y = C_{\text{acc}}x + D_{\text{acc}, u}u + D_{\text{acc}, d}d, \quad (14)$$

where

$$C_{\text{acc}} \triangleq \begin{bmatrix} 0_{1 \times n_b} & e_{n_b, i_y}^T \end{bmatrix} A, \quad D_{\text{acc}, u} \triangleq \begin{bmatrix} 0_{1 \times n_b} & e_{n_b, i_y}^T \end{bmatrix} B_u, \quad D_{\text{acc}, d} \triangleq \begin{bmatrix} 0_{1 \times n_b} & e_{n_b, i_y}^T \end{bmatrix} B_d.$$

The LP system considered in this manuscript is single-input, single-output (SISO). The control objective for the LP system is to minimize the oscillations of w_{i_y} , propagated by the disturbance signal d by modulating the input signal u , which is determined by a control algorithm based on the measurement signal, which can be a displacement measurement w_{i_y} or an acceleration measurement \ddot{w}_{i_y} .

III. Control

In this section, the adaptive control algorithm and its implementation are introduced. Subsection III.A provides a review of Retrospective Cost Adaptive Control (RCAC), a discrete-time, model-free, adaptive control algorithm. Subsection III.C introduces the sampled-data implementation of RCAC to interface the discrete-time controller with the continuous-time system. Subsection III.D provides an overview of the signal conditioning filters used to improve the performance of the adaptive controller.

A. Review of Retrospective Cost Adaptive Control

RCAC is described in detail in [32]. In this subsection, we summarize the main elements of this method. Consider the strictly proper, discrete-time, input-output controller

$$u_{c,k} = \sum_{i=1}^{l_c} P_{i,k} u_{k-i} + \sum_{i=1}^{l_c} Q_{i,k} z_{k-i}, \quad (15)$$

where $u_{c,k} \in \mathbb{R}^{l_u}$ is the commanded input and the controller output $u_k \in \mathbb{R}^{l_u}$ is the control input, $z_k \in \mathbb{R}^{l_z}$ is the measured performance variable, l_c is the controller-window length, and, for all $i \in \{1, \dots, l_c\}$, $P_{i,k} \in \mathbb{R}^{l_u \times l_u}$ and $Q_{i,k} \in \mathbb{R}^{l_u \times l_z}$ are the controller coefficient matrices. Note that u_k results from applying constraints to $u_{c,k}$, as shown in Subsection III.C. The controller (15) can be written as

$$u_{c,k} = \phi_k \theta_k, \quad (16)$$

where

$$\phi_k \triangleq [u_{k-1}^T \dots u_{k-l_c}^T z_{k-1}^T \dots z_{k-l_c}^T] \otimes I_{l_u} \in \mathbb{R}^{l_u \times l_\theta}, \quad (17)$$

$$\theta_k \triangleq \text{vec} [P_{1,k} \dots P_{l_c,k} Q_{1,k} \dots Q_{l_c,k}] \in \mathbb{R}^{l_\theta}, \quad (18)$$

$l_\theta \triangleq l_c l_u (l_u + l_z)$, and θ_k is the vector of controller coefficients, which are updated at each time step k . If z_k and u_k are scalar, then the SISO transfer function of (15) from z_k to u_k is given by

$$G_{c,k}(\mathbf{q}) = \frac{Q_{1,k} \mathbf{q}^{l_c-1} + \dots + Q_{l_c,k}}{\mathbf{q}^{l_c} - P_{1,k} \mathbf{q}^{l_c-1} - \dots - P_{l_c,k}}. \quad (19)$$

Next, define the retrospective cost variable

$$\hat{z}_k(\hat{\theta}) \triangleq z_k - G_f(\mathbf{q})(u_k - \phi_k \hat{\theta}), \quad (20)$$

where G_f is an $l_z \times l_u$ asymptotically stable, strictly proper transfer function, and $\hat{\theta} \in \mathbb{R}^{l_\theta}$ is the controller coefficient vector determined by optimization below. The rationale underlying (20) is to replace the applied past control inputs with the re-optimized control input $\phi_k \hat{\theta}$ so that the closed-loop transfer function from $u_k - \phi_k \theta_{k+1}$ to z_k matches G_f [32, 46]. Consequently, G_f serves as a closed-loop target model for adaptation.

The filter G_f is called the *target model* and has the form

$$G_f(\mathbf{q}) \triangleq D_f^{-1}(\mathbf{q}) N_f(\mathbf{q}), \quad (21)$$

where D_f is an $l_z \times l_z$ polynomial matrix with leadin coefficient I_{l_u} , and N_f is an $l_z \times l_u$ polynomial matrix. By defining the filtered variables $\phi_{f,k} \in \mathbb{R}^{l_z \times l_\theta}$ and $u_{f,k} \in \mathbb{R}^{l_z}$, (20) can be written as

$$\hat{z}_k(\hat{\theta}) = z_k - (u_{f,k} - \phi_{f,k} \hat{\theta}), \quad (22)$$

where

$$\phi_{f,k} \triangleq G_f(\mathbf{q}) \phi_k, \quad u_{f,k} \triangleq G_f(\mathbf{q}) u_k. \quad (23)$$

The choice of G_f includes all required modeling information. When the plant is SISO, that is, $l_z = l_u = 1$, this information consists of the sign of the leading numerator coefficient, the relative degree of the sampled-data system, and all nonminimum-phase (NMP) zeros [32, 46]. Since zeros are invariant under feedback, omission of a NMP zero from G_f may entail unstable pole-zero cancellation. Cancellation can be prevented, however, by using the control weighting R_u introduced below, as discussed in [32, 47]. G_f can be constructed and updated online using data [46]. For simplicity in controlling the LP model, which is a SISO system, we fix G_f prior to implementation.

Using (20), we define the cumulative cost function

$$J_k(\hat{\theta}) \triangleq \sum_{i=0}^k [\hat{z}_i^T(\hat{\theta}) \hat{z}_i(\hat{\theta}) + (\phi_i \hat{\theta})^T R_u \phi_i \hat{\theta}] + (\hat{\theta} - \theta_0)^T P_0^{-1} (\hat{\theta} - \theta_0), \quad (24)$$

where $P_0 \in \mathbb{R}^{l_\theta \times l_\theta}$ is positive definite, and $R_u \in \mathbb{R}^{l_u \times l_u}$ is positive semidefinite. As can be seen from (16), R_u serves as a control weighting, which prevents RCAC from cancelling unmodeled NMP zeros, and the matrix P_0^{-1} defines the regularization term and initializes the recursion for P_k defined below.

The following result uses recursive least squares (RLS) [48, 49] to minimize (24), where, at each step k , the minimizer of (24) is the update θ_{k+1} of the controller coefficient vector.

Proposition 1. For all $k \geq 0$, the unique global minimizer θ_{k+1} of (24) is given by

$$P_{k+1} = P_k - P_k \begin{bmatrix} \phi_{f,k} \\ \phi_k \end{bmatrix}^T \Gamma_k \begin{bmatrix} \phi_{f,k} \\ \phi_k \end{bmatrix} P_k, \quad (25)$$

$$\theta_{k+1} = \theta_k - P_{k+1} \begin{bmatrix} \phi_{f,k} \\ \phi_k \end{bmatrix}^T \bar{R} \begin{bmatrix} z_k - (u_{f,k} - \phi_{f,k} \theta_k) \\ \phi_k \theta_k \end{bmatrix}, \quad (26)$$

where

$$\Gamma_k \triangleq \bar{R} - \bar{R} \begin{bmatrix} \phi_{f,k} \\ \phi_k \end{bmatrix} \left(P_k^{-1} + \begin{bmatrix} \phi_{f,k} \\ \phi_k \end{bmatrix}^T \bar{R} \begin{bmatrix} \phi_{f,k} \\ \phi_k \end{bmatrix} \right)^{-1} \begin{bmatrix} \phi_{f,k} \\ \phi_k \end{bmatrix}^T \bar{R} \in \mathbb{R}^{(l_z+l_u) \times (l_z+l_u)}, \quad (27)$$

$$\bar{R} \triangleq \text{diag}(I_{l_z}, R_u) \in \mathbb{R}^{(l_z+l_u) \times (l_z+l_u)}. \quad (28)$$

For all of the numerical simulations and physical experiments in this paper, θ_k is initialized as $\theta_0 = 0_{l_\theta \times 1}$ to reflect the absence of additional prior modeling information. For convenience, we set $P_0 = p_0 I_{l_\theta}$, where the scalar $p_0 > 0$ determines the initial rate of adaptation.

B. Target model G_f for systems with sinusoidal disturbances and time delays

The structure of G_f can be designed to account for sinusoidal disturbances and time delays. Note that time delays can also be induced by linear, time-invariant systems in applications that involve signals with sinusoidal components. In this case, G_f is given by

$$G_f(\mathbf{q}) = \frac{N}{\mathbf{q}^{d_f}} \left(\frac{1}{\mathbf{q}^2 - 2\alpha_f \cos(\omega_f T_s) \mathbf{q} + \alpha_f^2} \right) \quad (29)$$

where $N \in \{-1, 1\}$ encodes the sign of the leading coefficient corresponding to the system model, $d_f \geq 0$ is an integer that encodes the system time-delay, $\omega_f \triangleq 2\pi f_f$, where $f_f > 0$ encodes the disturbance frequency, and $\alpha_f \in (0, 1]$ determines how close the eigenvalues of G_f are to the unit circle circumference. In the case where $\alpha_f = 1$, the eigenvalues of G_f are placed at the unit circle circumference and for all $\alpha_f < 1$ the eigenvalues are placed inside the unit circle. While values of α_f closer to 1 yield better disturbance rejection results, this can result in numerical instability. Furthermore, the sign of N can be inverted to account for a phase delay of π rad, which can be used in cases where acceleration measurements are considered.

C. Sampled-data Controller Implementation

The adaptive controller is implemented as a sampled-data controller. Figure 3 shows a block diagram of the sampled-data closed-loop system, where $y \in \mathbb{R}$ is the output of the continuous-time system \mathcal{M} , y_k is the sampled output, $r_k \in \mathbb{R}$ is the discrete-time command, $e_k \triangleq r_k - y_k$ is the command-following error, and $T_s > 0$ is the controller sampling period. The digital-to-analog (D/A) and analog-to-digital (A/D) interfaces, which are synchronous, are zero-order-hold (ZOH) and sampler, respectively. For this work, $r \equiv 0$ reflects the desire to suppress oscillations in the measured signal. Finally, \mathcal{M} represents the LP model introduced in Section II.

The measured performance variable z_k , which is used for adaptation, is the output of filter \mathcal{F} , which is used for signal conditioning. The form of filter \mathcal{F} depends on whether the available measurement y is a displacement or an acceleration, and more details are provided in Subsection III.D. The adaptive controller $G_{c,k}$ operates on z_k to produce the discrete-time control $u_{c,k} \in \mathbb{R}$. Hence, $l_u = l_z = 1$. Since the response of a real actuator is subjected to hardware constraints, the implemented discrete-time control is $u_k \triangleq \sigma(u_{c,k})$, where $\sigma: \mathbb{R} \rightarrow \mathbb{R}$ is the control-magnitude saturation function

$$\sigma(u) \triangleq \begin{cases} u_{\max}, & u > u_{\max}, \\ u, & u_{\min} \leq u \leq u_{\max}, \\ u_{\min}, & u < u_{\min}, \end{cases} \quad (30)$$

where $u_{\min}, u_{\max} \in \mathbb{R}$ are the lower and upper magnitude saturation levels, respectively. $G_{c,k}, u_{c,k}$, and u_k are updated at each sampling time $t_k \stackrel{\Delta}{=} kT_s$. Implementation of the adaptive controller requires selection of the hyperparameters l_c , p_0 , and R_u depending on the system and performance requirements. Note that R_u is scalar since $l_u = 1$.

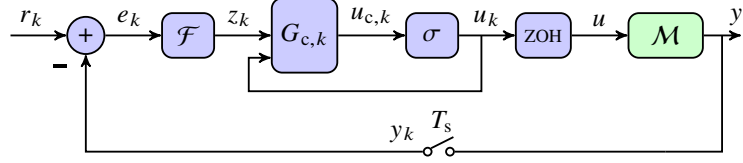


Fig. 3 Sampled-data implementation of adaptive controller for control of the continuous-time system \mathcal{M} . For this work, $r \equiv 0$ reflects the desire to minimize the oscillations in the measured signal, \mathcal{F} is a filter for signal conditioning, σ is the control-magnitude saturation, and \mathcal{M} represents the LP model introduced in Section II. The form of filter \mathcal{F} depends on whether the available measurement y is a displacement or an acceleration, and more details are given in Subsection III.D.

D. Filter for Signal Conditioning

The signal conditioning filter \mathcal{F} introduced in Subsection III.C is used for improved suppression performance and its form depends on whether the available measurement is a displacement or an acceleration. Three filters are considered depending on the available measurements.

In the case where displacement measurements are available, \mathcal{F} takes the form of a gain since displacement measurements in vibrational systems are small in magnitude; the filter is given by

$$\mathcal{F} = K_g, \quad (31)$$

where $K_g > 0$.

In the case where only acceleration measurements are available, we consider two filters with the objective of minimizing the magnitude of higher frequencies in the four acceleration signals that may be excited by the controller. The first filter is a *low-pass filter* that yields a filtered acceleration signal, and is given by

$$\mathcal{F} = \frac{K_g b_{lp} \mathbf{q}}{\mathbf{q}^2 + a_{lp,1} \mathbf{q} + a_{lp,2}}, \quad (32)$$

where

$$a_{lp,1} = -2r_{lp} \cos \theta_{lp}, \quad (33)$$

$$a_{lp,2} = r_{lp}^2, \quad (34)$$

$$b_{lp} = 1 + a_{lp,1} + a_{lp,2}, \quad (35)$$

$$r_{lp} = e^{-\zeta_{lp} \omega_{lp} T_s}, \quad (36)$$

$$\theta_{lp} = \omega_{lp} T_s \sqrt{1 - \zeta_{lp}^2}, \quad (37)$$

$K_g > 0$ is the filter gain, $\omega_{lp} > 0$ is the filter cutoff frequency, and $\zeta_{lp} \in (0, 1)$ is the filter damping. The second filter is a *displacement estimation filter* composed by cascaded high-pass filters and integrators, based on the technique shown in [50], that yield a pseudo-displacement estimate signal, and is shown in Figure 4, where $K_g > 0$ is the filter gain, and $\nu_{hp} > 0$ determines the high-pass filter cutoff frequency. Note that the high-pass filter is equivalent to the subtraction of the original signal minus the cumulative average of the signal, calculated using a window of length ν_{hp} .

IV. Numerical Simulations

In this section, we present the results of numerical simulations in which the RCAC algorithm is implemented to decrease the amplitude of the oscillations at a measurement point on the cantilever beam, caused by an external disturbance. The results for feedback control using displacement measurements and acceleration measurements with

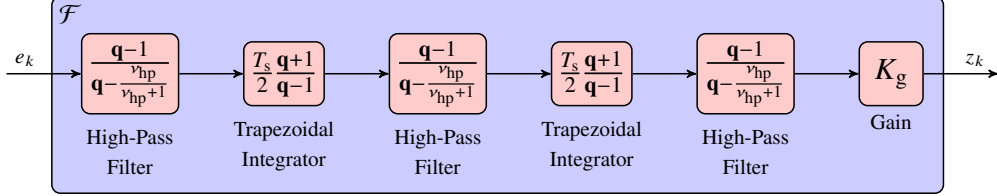


Fig. 4 Signal conditioning filter \mathcal{F} in which the input e_k is an acceleration measurement and the output z_k is a displacement estimate. $K_g > 0$ is the filter gain, and $v_{hp} > 0$ determines the high-pass filter cutoff frequency.

a low-pass filter and a displacement estimation filter are shown. In all cases, the open-loop results (no control) are compared to the closed-loop results (with feedback control), and RCAC is enabled at $t = 2.5$ s to allow the measured oscillations propagated by the disturbance enough time to settle.

For all numerical simulations, the simulation sampling period is $T_{\text{sim}} = 10^{-4}$ s and the controller sampling period is $T_s = 2.5 \times 10^{-3}$ s. The `ode45` solver from Matlab is used to integrate the model dynamics in between controller time steps.

The following cantilever system parameters are used:

$$L = 0.5 \text{ m}, \quad h = 0.05 \text{ m}, \quad b = 0.001 \text{ m}, \quad m = 0.07 \text{ kg}, \quad E = 69 \times 10^9 \text{ N/m}^2, \quad \alpha = 1.5 \text{ s}^{-1}, \quad \beta = 2.5 \times 10^{-4} \text{ s},$$

$$n_b = 20, \quad i_d = 5, \quad i_y = 20, \quad u_{\max} = -u_{\min} = 2.5,$$

where Young's modulus E is chosen considering aluminum as the material of the beam, and α and β are chosen so that the minimum damping ratio corresponding to the eigenvalues of A is approximately 0.1. It follows from the value of i_d and i_y that the disturbance signal is applied at the fourth of the beam near the clamped end, and the measurement signal is obtained from the unclamped end of the beam. Furthermore, for all $t \geq 0$, the disturbance signal is given by $d(t) = \sin(2\pi f_{\text{dist}} t)$, that is, a sinusoidal signal with unit amplitude and a frequency of f_{dist} Hz.

To test the effectiveness of RCAC under system parameter variations, the placement of the input i_u and the disturbance frequency f_{dist} are varied in different simulation runs, such that RCAC is tested under all combinations of $i_u \in \{10, 12, 14, 16\}$ and $f_{\text{dist}} = \{20, 40, 60, 80\}$ Hz. All tests are performed for each of the following cases:

- 1) Displacement measurement feedback (C_{disp}).
- 2) Acceleration measurement feedback with low-pass filter ($C_{\text{acc,lp}}$).
- 3) Acceleration measurement feedback with displacement estimation filter ($C_{\text{acc,disp est}}$).

For each of these cases, a set of hyperparameters is fixed for all simulation runs, and d_f and R_u are chosen for each i_u and f_{dist} combination to achieve the largest vibration attenuation, as these have the greatest impact on vibration attenuation performance. For all cases, the hyperparameters of the target model G_f other than d_f and N are fixed to $\omega_f = 2\pi f_f = 2\pi f_{\text{dist}}$ and $\alpha_f = 0.95$.

Furthermore, to quantify vibration attenuation performance, we define

$$y_{\text{disp,dec}} \triangleq \frac{y_{\text{disp,OL}}}{y_{\text{disp,CL}}}, \quad (38)$$

where $y_{\text{disp,OL}}$ is the steady-state amplitude of the displacement at i_y in the open-loop case and $y_{\text{disp,CL}}$ is the steady-state amplitude of the displacement at i_y in the closed-loop case. The simulations are run until the displacement amplitudes converge to a constant value; $y_{\text{disp,OL}}$ and $y_{\text{disp,CL}}$ are obtained as the maximum measured displacement amplitudes of the last 0.5 s of the simulation time.

A. Displacement Measurements

For RCAC implementation using displacement measurement feedback C_{disp} , the following hyperparameters are fixed for all simulation tests:

$$l_c = 20, \quad p_0 = 1, \quad N = -1, \quad u_{\max} = -u_{\min} = 2.5, \quad K_g = 500.$$

To illustrate the effectiveness of RCAC for vibration suppression, the results of this implementation in the case where $i_u = 12$ and $f_{\text{dist}} = 20$ Hz with $d_f = 5$ and $R_u = 1$ are shown in Figures 5, 6, and 7. In particular, it follows from Figure

5 that the resulting vibration attenuation is given by $y_{\text{disp,dec}} = 30.38$ dB. Finally, the vibration attenuation obtained in simulation runs under all combinations of $i_u \in \{10, 12, 14, 16\}$ and $f_{\text{dist}} = \{20, 40, 60, 80\}$ Hz is summarized in Table 1, which also include the choice of d_f and R_u used to obtain each result.

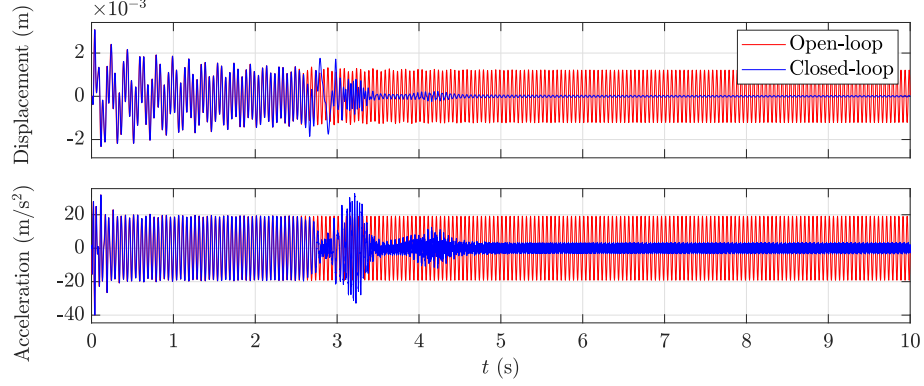


Fig. 5 Subsection IV.A: Open-loop and closed-loop displacement and acceleration results in the time domain with RCAC using displacement measurements C_{disp} in the case where $i_u = 12$ and $f_{\text{dist}} = 20$ Hz with $d_f = 5$ and $R_u = 1$.

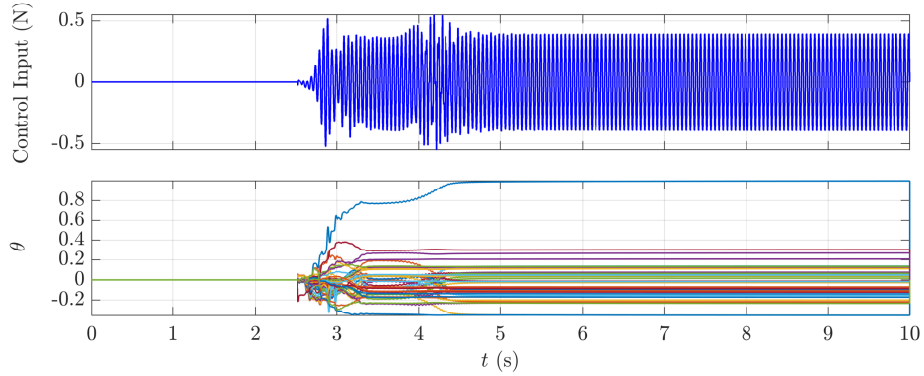


Fig. 6 Subsection IV.A: Control input and RCAC coefficients θ in the time domain with RCAC using displacement measurements C_{disp} in the case where $i_u = 12$ and $f_{\text{dist}} = 20$ Hz with $d_f = 5$ and $R_u = 1$.

Table 1 Subsection IV.A: Vibration attenuation results with RCAC using displacement measurements C_{disp} for all combinations of $i_u \in \{10, 12, 14, 16\}$ and $f_{\text{dist}} = \{20, 40, 60, 80\}$ Hz. The table displays the vibration attenuation $y_{\text{disp,dec}}$ defined in (38), and the hyperparameters d_f and R_u used to obtain these results.

| f_{dist} | i_u | Vibration attenuation $y_{\text{disp,dec}}$ (dB) | | | | d_f | | | | R_u | | | |
|-------------------|-------|--|-------|-------|-------|-------|----|----|----|-------|------|------|------|
| | | 10 | 12 | 14 | 16 | 10 | 12 | 14 | 16 | 10 | 12 | 14 | 16 |
| 20 Hz | 10 | 30.97 | 30.38 | 31.67 | 32.41 | 5 | 5 | 5 | 5 | 1 | 1 | 1 | 1 |
| 40 Hz | 10 | 28.78 | 27.88 | 4.16 | 26.97 | 9 | 8 | 7 | 3 | 0.5 | 0.4 | 0.5 | 0.4 |
| 60 Hz | 10 | 28.51 | 2.01 | 21.37 | 29.62 | 6 | 5 | 9 | 3 | 0.05 | 0.1 | 0.1 | 0.05 |
| 80 Hz | 10 | 8.30 | 21.39 | 28.00 | 27.34 | 9 | 7 | 7 | 7 | 0.1 | 0.05 | 0.05 | 0.05 |

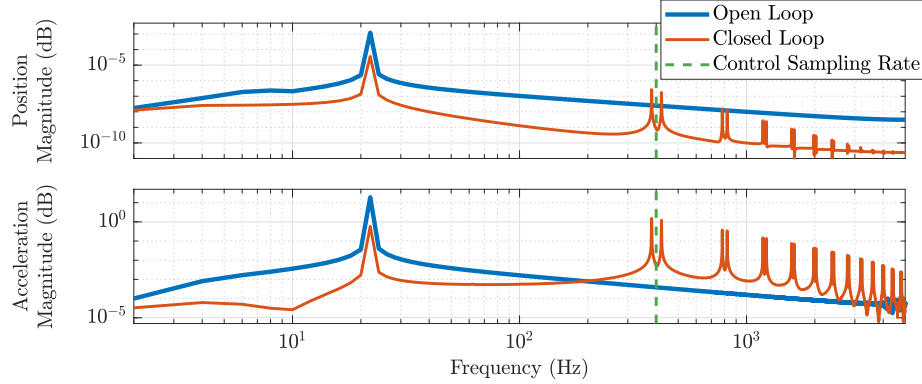


Fig. 7 Subsection IV.A: Open-loop and closed-loop displacement and acceleration results in the frequency domain with RCAC using displacement measurements C_{disp} in the case where $i_u = 12$ and $f_{\text{dist}} = 20$ Hz with $d_f = 5$ and $R_u = 1$.

B. Acceleration Measurements and Low-Pass Filter

For RCAC implementation using acceleration measurement feedback with a low-pass filter $C_{\text{acc,lp}}$, the following hyperparameters are fixed for all simulation tests:

$$l_c = 20, \quad p_0 = 1, \quad R_u = 40, \quad N = 1, \quad K_g = 1, \quad \omega_{\text{lp}} = 2\pi 150, \quad \zeta_{\text{lp}} = 0.8.$$

To illustrate the effectiveness of RCAC for vibration suppression, the results of this implementation in the case where $i_u = 12$ and $f_{\text{dist}} = 20$ Hz with $d_f = 5$ and $R_u = 1$ are shown in Figures 8, 9, and 10. In particular, it follows from Figure 8 that the resulting vibration attenuation is given by $y_{\text{disp,dec}} = 20.42$ dB. Finally, the vibration attenuation obtained in simulation runs under all combinations of $i_u \in \{10, 12, 14, 16\}$ and $f_{\text{dist}} \in \{20, 40, 60, 80\}$ Hz is summarized in Table 2, which also include the choice of d_f and R_u used to obtain each result.

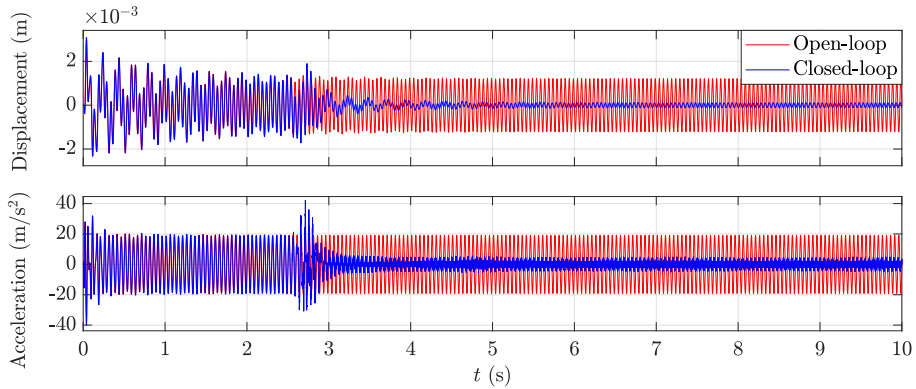


Fig. 8 Subsection IV.B: Open-loop and closed-loop displacement and acceleration results in the time domain with RCAC using acceleration measurements with a low-pass filter $C_{\text{acc,lp}}$ in the case where $i_u = 12$ and $f_{\text{dist}} = 20$ Hz with $d_f = 5$ and $R_u = 1$.

C. Acceleration Measurements and Displacement Estimation Filter

For RCAC implementation using acceleration measurement feedback with a displacement estimation filter $C_{\text{acc,disp est}}$, the following hyperparameters are fixed for all simulation tests:

$$l_c = 25, \quad p_0 = 0.1, \quad N = -1, \quad K_g = 500, \quad \nu_{\text{hp}} = 20.$$

To illustrate the effectiveness of RCAC for vibration suppression, the results of this implementation in the case where $i_u = 12$ and $f_{\text{dist}} = 20$ Hz with $d_f = 8$ and $R_u = 1$ are shown in Figures 11, 12, and 13. In particular, it follows from

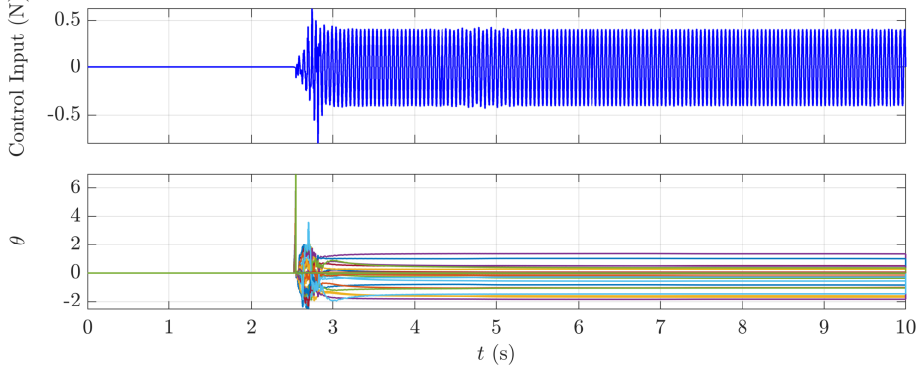


Fig. 9 Subsection IV.B: Control input and RCAC coefficients θ in the time domain with RCAC using acceleration measurements with a low-pass filter $C_{\text{acc},\text{lp}}$ in the case where $i_u = 12$ and $f_{\text{dist}} = 20$ Hz with $d_f = 5$ and $R_u = 1$.

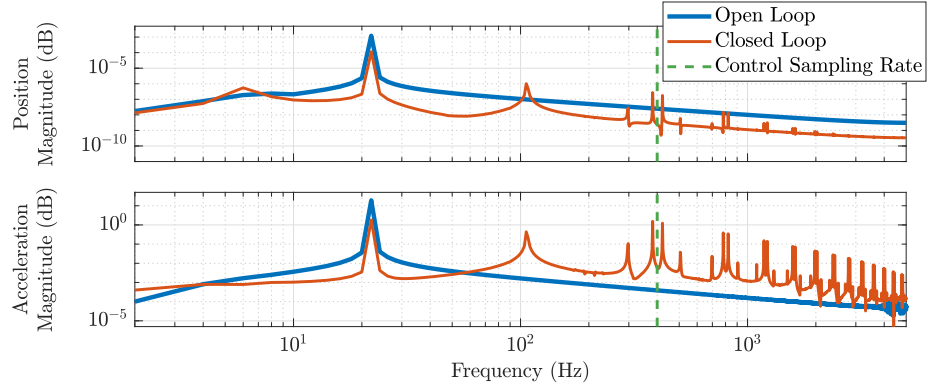


Fig. 10 Subsection IV.B: Open-loop and closed-loop displacement and acceleration results in the frequency domain with RCAC using acceleration measurements with a low-pass filter $C_{\text{acc},\text{lp}}$ in the case where $i_u = 12$ and $f_{\text{dist}} = 20$ Hz with $d_f = 5$ and $R_u = 1$.

Table 2 Subsection IV.B: Vibration attenuation results with RCAC using acceleration measurements with a low-pass filter $C_{\text{acc},\text{lp}}$ for all combinations of $i_u \in \{10, 12, 14, 16\}$ and $f_{\text{dist}} = \{20, 40, 60, 80\}$ Hz. The table displays the vibration attenuation $y_{\text{disp,dec}}$ defined in (38), and the hyperparameters d_f and R_u used to obtain these results.

| f_{dist} | i_u | Vibration attenuation $y_{\text{disp,dec}}$ (dB) | | | | d_f | | | | R_u | | | |
|-------------------|-------|--|-------|-------|-------|-------|----|----|----|-------|----|-----|----|
| | | 10 | 12 | 14 | 16 | 10 | 12 | 14 | 16 | 10 | 12 | 14 | 16 |
| 20 Hz | 10 | 30.27 | 20.42 | 16.07 | 22.81 | 3 | 3 | 3 | 3 | 40 | 40 | 30 | 30 |
| 40 Hz | 10 | 24.20 | 23.09 | 5.43 | 26.83 | 8 | 7 | 7 | 8 | 40 | 40 | 100 | 40 |
| 60 Hz | 10 | 21.67 | -2.37 | 6.49 | 26.14 | 9 | 20 | 20 | 18 | 60 | 1 | 50 | 50 |
| 80 Hz | 10 | 8.79 | 10.80 | 14.47 | 26.92 | 20 | 19 | 19 | 19 | 40 | 50 | 100 | 60 |

Figure 11 that the resulting vibration attenuation is given by $y_{\text{disp,dec}} = 26.77$ dB. Finally, the vibration attenuation obtained in simulation runs under all combinations of $i_u \in \{10, 12, 14, 16\}$ and $f_{\text{dist}} = \{20, 40, 60, 80\}$ Hz is summarized in Table 3, which also include the choice of d_f and R_u used to obtain each result.

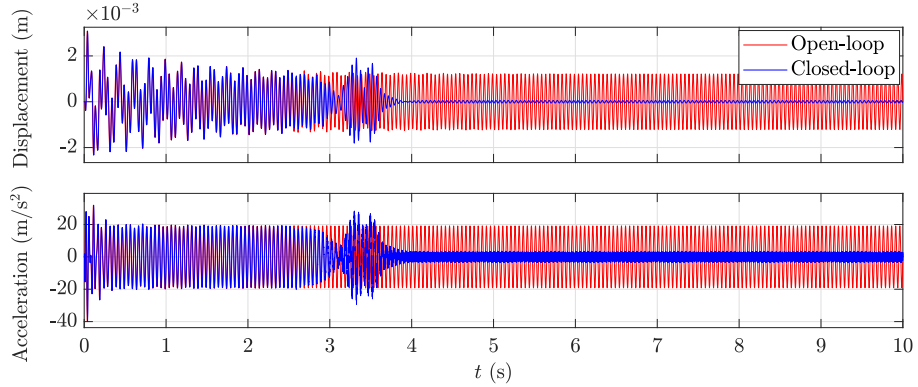


Fig. 11 Subsection IV.C: Open-loop and closed-loop displacement and acceleration results in the time domain with RCAC using acceleration measurements with a displacement estimation filter $C_{\text{acc,disp est}}$ in the case where $i_u = 12$ and $f_{\text{dist}} = 20$ Hz with $d_f = 5$ and $R_u = 1$.

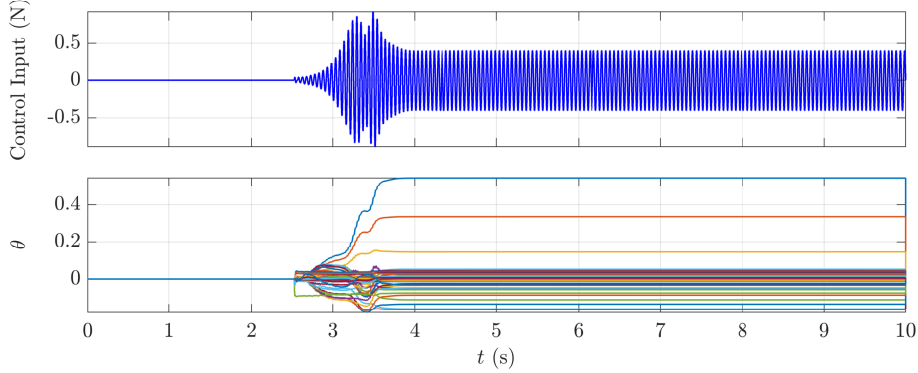


Fig. 12 Subsection IV.C: Control input and RCAC coefficients θ in the time domain with RCAC using acceleration measurements with a displacement estimation filter $C_{\text{acc,disp est}}$ in the case where $i_u = 12$ and $f_{\text{dist}} = 20$ Hz with $d_f = 5$ and $R_u = 1$.

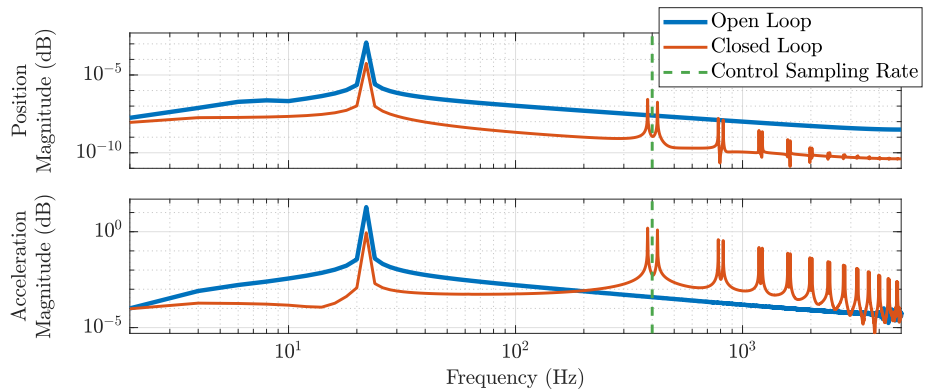


Fig. 13 Subsection IV.C: Open-loop and closed-loop displacement and acceleration results in the frequency domain with RCAC using acceleration measurements with a displacement estimation filter $C_{\text{acc,disp est}}$ in the case where $i_u = 12$ and $f_{\text{dist}} = 20$ Hz with $d_f = 5$ and $R_u = 1$.

Table 3 Subsection IV.C: Vibration attenuation results with RCAC using acceleration measurements with a displacement estimation filter $C_{\text{acc,disp est}}$ for all combinations of $i_u \in \{10, 12, 14, 16\}$ and $f_{\text{dist}} = \{20, 40, 60, 80\}$ Hz. The table displays the vibration attenuation $y_{\text{disp,dec}}$ defined in (38), and the hyperparameters d_f and R_u used to obtain these results.

| f_{dist} | i_u | Vibration attenuation $y_{\text{disp,dec}}$ (dB) | | | | d_f | | | | R_u | | | |
|-------------------|-------|--|-------|-------|----|-------|----|----|------|-------|------|------|----|
| | | 10 | 12 | 14 | 16 | 10 | 12 | 14 | 16 | 10 | 12 | 14 | 16 |
| 20 Hz | 27.19 | 26.77 | 23.49 | 28.85 | 3 | 8 | 8 | 8 | 1 | 1 | 5 | 1 | |
| 40 Hz | 26.18 | 28.47 | 4.10 | 25.90 | 8 | 5 | 6 | 5 | 0.05 | 0.5 | 2 | 0.75 | |
| 60 Hz | 14.30 | 0.81 | 20.19 | 21.90 | 6 | 5 | 4 | 9 | 0.1 | 1 | 0.75 | 0.05 | |
| 80 Hz | 8.16 | 9.54 | 15.20 | 27.02 | 9 | 7 | 8 | 8 | 0.05 | 0.1 | 0.1 | 0.1 | |

D. Comparison of closed-loop performance

The results of the three measurement and filter combinations (C_{disp} , $C_{\text{acc,lp}}$, $C_{\text{acc,disp est}}$) are summarized and compared in Figure 14. In most cases, $C_{\text{acc,disp est}}$ improves upon $C_{\text{acc,lp}}$. However, the performance of $C_{\text{acc,disp est}}$ deteriorates at higher frequencies ($f_{\text{dist}} \in \{60, 80\}$ Hz). Since displacement estimation filter hyperparameter ν_{hp} was chosen considering the case in which $f_{\text{dist}} = 20$ Hz, retuning ν_{hp} may be required for improved performance at higher frequencies. Hence, $C_{\text{acc,disp est}}$ offers the possibility of recovering the performance from displacement feedback C_{disp} .

Another advantage of $C_{\text{acc,disp est}}$ is that it possesses similar closed-loop behavior to C_{disp} . To illustrate this, note that the acceleration magnitude frequency response of the closed-loop result corresponding to $C_{\text{acc,lp}}$, shown in Figure 10, shows two more frequency peaks at frequencies lower than the control sampling frequency than the frequency peaks in the frequency responses corresponding to C_{disp} and $C_{\text{acc,disp est}}$, shown in Figures 7 and 13.

Finally, it follows from Tables 1, 2, and 3 that the optimal hyperparameters for $C_{\text{acc,disp est}}$ are closer to those corresponding to C_{disp} than those corresponding to $C_{\text{acc,lp}}$, especially in the cases where $f_{\text{dist}} \in \{60, 80\}$ Hz. Hence, the hyperparameter space considered for C_{disp} can also be used for $C_{\text{acc,disp est}}$.

V. Conclusions

This paper presented a lumped-parameter model of a cantilever beam and applied the retrospective cost adaptive control (RCAC) algorithm for suppressing vibrations induced by external sinusoidal disturbances, without requiring any prior model information of the beam. Numerical simulations demonstrate that RCAC can effectively attenuate vibration using both displacement and acceleration feedback. Simulation results indicate that displacement feedback provides superior closed-loop performance compared to acceleration feedback. However, in practical applications, acceleration measurements are significantly easier to obtain and more reliable than displacement measurements. While acceleration can be obtained directly from sensors or by differentiating displacement twice, the reverse process, that is, recovering displacement through double integration of acceleration, is generally infeasible due to uncertainty in the initial conditions. To address this limitation, a pseudo-displacement estimate was formulated by conditioning the acceleration measurements, as discussed in Section III.D. Results show that this pseudo-displacement feedback outperforms pure acceleration feedback at lower disturbance frequencies, whereas both approaches perform comparably at higher frequencies. Since the displacement-estimate filter was tuned primarily for lower-frequency disturbances, further performance gains are expected by optimizing the filter design for higher-frequency operation. Future work will focus on enhancing the pseudo-displacement feedback scheme and reducing the dependence of RCAC performance on hyperparameter tuning.

References

- [1] Alkhatib, R., and Golnaraghi, M., “Active structural vibration control: a review,” *Shock and Vibration Digest*, Vol. 35, No. 5, 2003, p. 367.
- [2] Vasques, C., and Rodrigues, J. D., “Active vibration control of smart piezoelectric beams: comparison of classical and optimal feedback control strategies,” *Computers & Structures*, Vol. 84, No. 22-23, 2006, pp. 1402–1414.

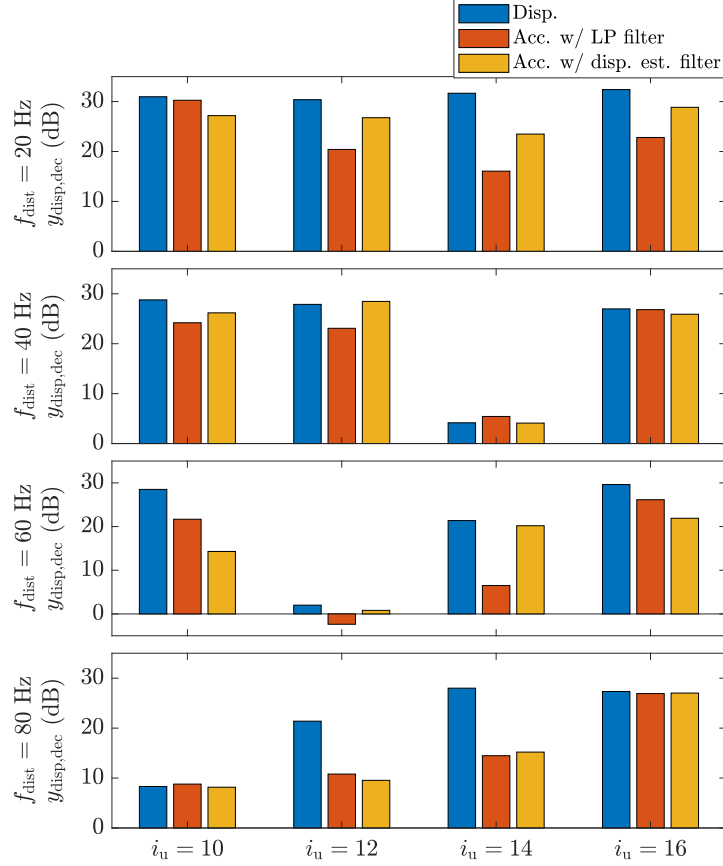


Fig. 14 Subsection IV.D: Vibration attenuation $y_{\text{disp,dec}}$ with RCAC using displacement measurements, acceleration measurements with a low-pass filter, and acceleration measurements with a displacement estimation filter. The results are shown for all combinations of $i_u \in \{10, 12, 14, 16\}$ and $f_{\text{dist}} = \{20, 40, 60, 80\}$ Hz.

- [3] Caresta, M., “Active control of sound radiated by a submarine in bending vibration,” *J. Sound Vib.*, Vol. 330, No. 4, 2011, pp. 615–624.
- [4] Aridogan, U., and Basdogan, I., “A review of active vibration and noise suppression of plate-like structures with piezoelectric transducers,” *J. Intell. Material Syst. Struct.*, Vol. 26, No. 12, 2015, pp. 1455–1476.
- [5] Preumont, A., *Vibration control of active structures: an introduction*, Vol. 246, Springer, 2018.
- [6] Cunha, B. Z., Droz, C., Zine, A.-M., Foulard, S., and Ichchou, M., “A review of machine learning methods applied to structural dynamics and vibroacoustic,” *Mech. Syst. Sig. Proc.*, Vol. 200, 2023, p. 110535.
- [7] Li, J., Zhang, L., Li, S., Mao, Q., and Mao, Y., “Active disturbance rejection control for piezoelectric smart structures: A review,” *Machines*, Vol. 11, No. 2, 2023, p. 174.
- [8] Daley, S., Johnson, F., Pearson, J., and Dixon, R., “Active vibration control for marine applications,” *Contr. Eng. Pract.*, Vol. 12, No. 4, 2004, pp. 465–474.
- [9] Zhang, B.-L., Han, Q.-L., and Zhang, X.-M., “Recent advances in vibration control of offshore platforms,” *Nonlin. Dyn.*, Vol. 89, 2017, pp. 755–771.
- [10] Soni, T., Das, A., and Dutt, J., “Active vibration control of ship mounted flexible rotor-shaft-bearing system during seakeeping,” *J. Sound Vib.*, Vol. 467, 2020, p. 115046.
- [11] Shiba, K., Mase, S., Yabe, Y., and Tamura, K., “Active/passive vibration control systems for tall buildings,” *Smart Materials Struct.*, Vol. 7, No. 5, 1998, p. 588.

[12] Li, A., *Vibration control for building structures*, Springer, Cham, Switzerland, 2020.

[13] Ramírez-Neria, M., Morales-Valdez, J., and Yu, W., “Active vibration control of building structure using active disturbance rejection control,” *J. Vib. Contr.*, Vol. 28, No. 17-18, 2022, pp. 2171–2186.

[14] Hu, Q., and Ma, G., “Variable structure control and active vibration suppression of flexible spacecraft during attitude maneuver,” *Aerosp. Sci. Tech.*, Vol. 9, No. 4, 2005, pp. 307–317.

[15] Hu, Q., “Variable structure maneuvering control with time-varying sliding surface and active vibration damping of flexible spacecraft with input saturation,” *Acta Astronautica*, Vol. 64, No. 11-12, 2009, pp. 1085–1108.

[16] He, W., and Ge, S. S., “Dynamic modeling and vibration control of a flexible satellite,” *IEEE Trans. Aerosp. Electron. Sys.*, Vol. 51, No. 2, 2015, pp. 1422–1431.

[17] Tsushima, N., and Su, W., “A study on adaptive vibration control and energy conversion of highly flexible multifunctional wings,” *Aerosp. Sci. Tech.*, Vol. 79, 2018, pp. 297–309.

[18] Prakash, S., Kumar, T. R., Raja, S., Dwarakanathan, D., Subramani, H., and Karthikeyan, C., “Active vibration control of a full scale aircraft wing using a reconfigurable controller,” *J. Sound Vib.*, Vol. 361, 2016, pp. 32–49.

[19] Bloemers, T., Leemrijse, S., Preda, V., Boquet, F., Oomen, T., and Tóth, R., “Vibration Control Under Frequency-Varying Disturbances With Application to Satellites,” *IEEE Trans. Contr. Sys. Tech.*, 2024.

[20] Zhang, J., He, L., Wang, E., and Gao, R., “A LQR controller design for active vibration control of flexible structures,” *Proc. Pacific-Asia Workshop Comp. Intell. Indust. Appl.*, Vol. 1, IEEE, 2008, pp. 127–132.

[21] Schulz, S. L., Gomes, H. M., and Awruch, A. M., “Optimal discrete piezoelectric patch allocation on composite structures for vibration control based on GA and modal LQR,” *Comp. Struct.*, Vol. 128, 2013, pp. 101–115.

[22] Zhang, H., Sun, W., Luo, H., and Zhang, R., “Active vibration control of composite laminates with MFC based on PID-LQR hybrid controller,” *Mech. Adv. Materials Struct.*, Vol. 31, No. 25, 2024, pp. 6382–6399.

[23] Souza, A. G., and Souza, L., “Design of a controller for a rigid-flexible satellite using the H-infinity method considering the parametric uncertainty,” *Mech. Sys. Sig. Proc.*, Vol. 116, 2019, pp. 641–650.

[24] Fan, L., Huang, H., Sun, L., and Zhou, K., “Robust attitude control for a rigid-flexible-rigid microsatellite with multiple uncertainties and input saturations,” *Aerosp. Sci. Tech.*, Vol. 95, 2019, p. 105443.

[25] Wang, Z., Wu, W., Görge, D., and Lou, X., “Sliding mode vibration control of an Euler–Bernoulli beam with unknown external disturbances,” *Nonl. Dyn.*, Vol. 110, No. 2, 2022, pp. 1393–1404.

[26] Qiu, J., and Haraguchi, M., “Vibration control of a plate using a self-sensing piezoelectric actuator and an adaptive control approach,” *J. Intell. Material Sys. Struct.*, Vol. 17, No. 8-9, 2006, pp. 661–669.

[27] Landau, I. D., “On the use of Youla–Kucera parametrisation in adaptive active noise and vibration control—a review,” *Int. J. Contr.*, Vol. 93, No. 2, 2020, pp. 204–216.

[28] Batista, E. L. O., Barghouthi, M. R., and de Oliveira Lopes, E. M., “A novel adaptive scheme to improve the performance of feedforward active vibration control systems,” *IEEE/ASME Trans. Mechatron.*, Vol. 27, No. 4, 2021, pp. 2322–2332.

[29] Saeed, M. U., Sun, Z., and Elias, S., “Research developments in adaptive intelligent vibration control of smart civil structures,” *J. Low Freq. Noise Vib. Active Contr.*, Vol. 41, No. 1, 2022, pp. 292–329.

[30] Wang, M., Fang, X., Wang, Y., Ding, J., Sun, Y., Luo, J., and Pu, H., “A dual-loop active vibration control technology with an RBF-RLS adaptive algorithm,” *Mech. Sys. Sig. Proc.*, Vol. 191, 2023, p. 110079.

[31] Liu, T., Liu, C., and Zhang, Z., “Adaptive active vibration control for composite laminated plate: theory and experiments,” *Mech. Sys. Sig. Proc.*, Vol. 206, 2024, p. 110876.

[32] Rahman, Y., Xie, A., and Bernstein, D. S., “Retrospective Cost Adaptive Control: Pole Placement, Frequency Response, and Connections with LQG Control,” *IEEE Contr. Sys. Mag.*, Vol. 37, 2017, pp. 28–69.

[33] Mohseni, N., and Bernstein, D. S., “Retrospective cost adaptive harmonic disturbance rejection using dereverberated target models,” *J. Sound Vib.*, Vol. 523, 2022, p. 116692.

[34] Paredes, J., Islam, S. A. U., and Bernstein, D. S., “Adaptive stabilization of thermoacoustic oscillations in a Rijke tube,” *Proc. Amer. Contr. Conf.*, IEEE, 2022, pp. 28–33.

[35] Paredes, J. A., and Bernstein, D. S., “Experimental implementation of retrospective cost adaptive control for suppressing thermoacoustic oscillations in a Rijke tube,” *IEEE Trans. Contr. Sys. Tech.*, Vol. 31, No. 6, 2023, pp. 2484–2498.

[36] Balas, M., “Trends in large space structure control theory: Fondest hopes, wildest dreams,” *IEEE Trans. Automat. Contr.*, Vol. 27, No. 3, 1982, pp. 522–535.

[37] Hyland, D., Junkins, J., and Longman, R., “Active control technology for large space structures,” *J. Guid. Contr. Dyn.*, Vol. 16, No. 5, 1993, pp. 801–821.

[38] Hong, J., and Bernstein, D. S., “Bode integral constraints, collocation, and spillover in active noise and vibration control,” *IEEE Trans. Contr. Syst. Tech.*, Vol. 6, No. 1, 1998, pp. 111–120.

[39] Dong, X., Peng, Z., Zhang, W., Hua, H., and Meng, G., “Research on spillover effects for vibration control of piezoelectric smart structures by ANSYS,” *Math. Prob. Eng.*, Vol. 2014, No. 1, 2014, p. 870940.

[40] Zhu, W.-H., Tryggvason, B., and Piedboeuf, J.-C., “On active acceleration control of vibration isolation systems,” *Contr. Eng. Pract.*, Vol. 14, No. 8, 2006, pp. 863–873.

[41] An, F., Chen, W.-d., and Shao, M.-q., “Study on discrete acceleration feedback control with time delay,” *J. Vib. Contr.*, Vol. 21, No. 7, 2015, pp. 1267–1285.

[42] Mounesisohi, A., and Bashash, S., “Vibration compensation of display contents in smart devices using accelerometer feedback,” *Proc. Conf. Contr. Tech. Appl.*, IEEE, 2017, pp. 420–425.

[43] Wei, L., Mengde, Z., Zhengquan, W., Zhuang, Y., Yu, L., Shihong, W., Xiaochun, C., Xiao, L., Zhenyuan, J., et al., “An active damping vibration control system for wind tunnel models,” *Chinese J. Aero.*, Vol. 32, No. 9, 2019, pp. 2109–2120.

[44] Huang, Y., Chen, W., and Shao, M., “Time-Delayed Acceleration Feedback Control of a Single-Link Flexible Manipulator Using Kalman Filter,” *Shock and Vibration*, Vol. 2021, No. 1, 2021, p. 6699145.

[45] Tůma, J., and Škutová, J., “Simulation of active vibration control of the cantilever beam,” *Proc. Int. Carpathian Contr. Conf.*, IEEE, 2012, pp. 744–747.

[46] Islam, S. A. U., Nguyen, T., Kolmanovsky, I., and Bernstein, D. S., “Data-Driven Retrospective Cost Adaptive Control for Flight Control Applications,” *J. Guid. Contr. Dyn.*, Vol. 44, 2021, pp. 1732–1758.

[47] Sumer, E. D., and Bernstein, D. S., “Retrospective cost adaptive control with error-dependent regularization for MIMO systems with uncertain nonminimum-phase transmission zeros,” *Proc. AIAA Guid. Nav. Contr. Conf.*, 2012, p. 4670. AIAA-2012-4670-123.

[48] Ljung, L., and Soderstrom, T., *Theory and Practice of Recursive Identification*, MIT Press, 1983.

[49] Islam, S. A. U., and Bernstein, D. S., “Recursive Least Squares for Real-Time Implementation,” *IEEE Contr. Syst. Mag.*, Vol. 39, No. 3, 2019, pp. 82–85.

[50] Zheng, W., Dan, D., Cheng, W., and Xia, Y., “Real-time dynamic displacement monitoring with double integration of acceleration based on recursive least squares method,” *Measurement*, Vol. 141, 2019, pp. 460–471.